Temperature dependence of ferromagnet-antiferromagnet spin alignment and coercivity in epitaxial micromagnet bilayers

Michael S. Lee, Thomas A. Wynn, Erik Folven, Rajesh V. Chopdekar, Andreas Scholl, Scott T. Retterer, Jostein K. Grepstad, and Yayoi Takamura

Phys. Rev. Materials **1**, 014402 — Published 26 June 2017

DOI: 10.1103/PhysRevMaterials.1.014402

Temperature Dependence of Ferromagnet-Antiferromagnet Spin Alignment and Coercivity in Epitaxial Micromagnet Bilayers

Michael S. Lee[1], Thomas A. Wynn[1], Erik Folven[2], Rajesh V. Chopdekar[1], Andreas Scholl[3], Scott T. Retterer[4], Jostein K. Grepstad[2], Yayoi Takamura[1]*

[1]Department of Materials Science and Engineering, University of California, Davis, Davis, CA 95616
[2]Department of Electronics and Telecommunications, Norwegian University of Science and Technology, NO-7491 Trondheim, Norway
[3]Advanced Light Source, Lawrence Berkeley National Laboratory, Berkeley, CA 94703
[4]Center for Nanophase Materials Sciences, Oak Ridge National Laboratory, Oak Ridge, TN 37831

Abstract

Soft x-ray photoemission electron microscopy with an *in situ* magnetic field has been used to study the relationship between ferromagnetic and antiferromagnetic spin alignment and the switching/reversal field of epitaxial micromagnetic structures. We investigated a model system consisting of a bilayer of ferromagnetic $La_{0.7}Sr_{0.3}MnO_3$ and antiferromagnetic $LaFeO_3$ where the spin axes in each layer can be driven from mutually perpendicular (spin-flop) to parallel alignment by varying the temperature between 30 K and 300 K. Results show that not only does this spin alignment noticeably influence the bilayer micromagnet coercivity compared to $La_{0.7}Sr_{0.3}MnO_3$ single-layer micromagnets, but the coercivity within this materials system can be tuned over a wide range by careful balance of material properties.

Introduction

Exchange coupling at the interface between ferromagnetic (FM) and antiferromagnetic (AFM) materials has immense technological significance (*1*). Implementation of magnetically coupled interfaces into devices typically requires patterning of thin films into micro- or nanoscale features, but it is often seen that the properties of fabricated systems differ from those of thin films. For example, it has long been known that coercivity, the external field required to switch a magnetic bit in the opposite direction, increases with decreasing FM particle dimension, but rapidly decreases once the superparamagnetic regime is reached (*2*). The exchange bias field between FM and AFM layers that imposes a unidirectional

anisotropy on the FM layer can be used to further modify magnetic switching (*1*). This interaction has been studied experimentally in microstructures, and results show that the magnitude of the bias field may be reduced by patterning. However, the origin of the size dependence is less clear (*3*). An epitaxial exchange coupled system introduces crystallographic dependence of the coupling behavior that is not present in polycrystalline designs. The interface between AFM $LaFeO_3$ (LFO) and FM $La_{0.7}Sr_{0.3}MnO_3$ (LSMO) is one intriguing example when these materials are grown epitaxially on (001)-oriented $SrTiO_3$ (STO) substrates. LFO is a G-type antiferromagnetic material (*4*) which produces a fully compensated (001) surface of Fe^{3+} moments. Heisenberg modeling predicts such an interface would align the FM and AFM spin-axes perpendicular to one another – a spin configuration known as spin-flop coupling (*5, 6*). Folven *et al.* verified this arrangement to be the energetically preferred coupling, yet in patterned bilayer films, a transition exists between spin-flop and parallel alignment as a function of both micromagnet aspect ratio and crystallographic orientation of the patterned structures (*7*). Understanding the influence of these parameters in micromagnetic structures is critical for device design and suggests that a wide range of magnetic behavior can be tuned within a single material system.

Subsequent work on LFO/LSMO bilayers characterized the switching behavior of 2 μm × 0.5 μm patterned micromagnets oriented along the in-plane <100> directions and demonstrated that parallel spin alignment reduces the switching field relative to a patterned LSMO single-layer (*8*). This decreased coercivity occurred since the AFM and FM moments prefer perpendicular alignment with one another. Thus, when switching the direction of the FM moment by 180°, the midpoint of the rotation of the FM magnetization becomes less unfavorable, thereby reducing the energetic barrier to switching.

Here, we demonstrate that the FM/AFM spin alignment in <110>-oriented epitaxial micromagnets is highly temperature dependent and that it is possible to stabilize different FM/AFM spin alignments. Relying on element specific domain imaging, we show that parallel, frustrated, and spin-flop states can be reached by varying the temperature between 300 K and 30 K within the same micromagnet array. This

fluctuation stems from the vastly different ordering temperatures (T_N = 670 K (*9*) for LFO and T_C = 270 K (*7*) for LSMO) of the individual layers. A Stoner-Wohlfarth free energy model developed to quantify the bias field imposed on the LSMO layer by the adjacent LFO layer predicts (relative to an LSMO single-layer) an increased switching field in spin-flop systems, reduced in the parallel configuration, and no change in the frustrated case (*i.e.* one with an equal mix of spin-flop and parallel aligned AFM domains within a single micromagnet). By applying *in-situ* field pulses, we test this model and also show that crystallographic orientation alone has considerable influence on the micromagnet coercivity. In total, this work demonstrates the variety of switching behavior that can be obtained in bit-patterned micromagnets through the combination of exchange-coupled systems with patterning of epitaxial multilayer films.

Methods and Materials

Two patterned epitaxial films were investigated in this work. The first was a 100 unit cell (u.c.) thick LSMO layer and the other was a bilayer consisting of 10 u.c. LFO grown on top of 90 u.c. LSMO. The samples were deposited by pulsed laser deposition on (001)-oriented Nb-doped (0.05 wt%) STO substrates. The growth and structural characterization were previously described in reference (*8*), and the films showed excellent crystalline and epitaxial quality. Within each film, microstructures are defined by a Cr hard mask using electron-beam lithography. A subsequent flood implantation of Ar^+ ions modifies the crystalline structure throughout the film thickness in all exposed regions, thus locally eliminating the magnetic order. This technique results in micromagnets embedded within a non-magnetic matrix. According to Stopping and Range of Ions in Matter simulations, implantation straggle does not appreciably modify the structural or magnetic quality of the microstructure beyond 30 nm of the pattern edge (*10*). More details on this patterning process can be found in references (*11*) and (*12*). The first of two microstructures discussed in this study are zig-zag patterns with 2 μm × 0.5 μm segments oriented along alternating in-plane <110> directions, and were measured between 30-300 K to evaluate the temperature dependence of the FM/AFM spin alignment. Arrays of ~100 2 μm × 0.5 μm rectangular bits,

oriented along the in-plane <110> direction, were also patterned into both films to study the magnetic switching behavior of these micromagnets.

X-ray photoemission electron microscopy (X-PEEM) was used to image the AFM and FM domains as a function of temperature between 30 K and 300 K at the PEEM3 endstation on beamline 11.0.1 at the Advanced Light Source (*13*). For these samples, FM domain contrast in X-PEEM emerges from x-ray magnetic circular dichroism (XMCD) at the Mn L_3 absorption edge, where the contrast intensity is proportional to the cosine of the angle between local FM moment orientation and the incident x-ray helicity vector. AFM domain images were obtained by utilizing the x-ray magnetic linear dichroism (XMLD) effect at the Fe L_2 absorption edge which is parametrized by $I(\theta) = a + b(3cos^2\theta - 1)\langle L^2\rangle$, where a and b are constants, $\boldsymbol{L}$ is the AFM moment, and θ is the angle between $\boldsymbol{L}$ and the $\boldsymbol{E}$-vector of the linearly polarized x-rays (*9*). X-PEEM images were collected with the x-ray $\boldsymbol{E}$-vector oriented along the [110] direction at two energies corresponding to the two local maxima of the Fe L_2 absorption edge. It has been shown that these energies possess opposite sign in the XMLD spectra (*14*). In order to enhance the AFM domain contrast and to eliminate any topographical contrast, the final AFM domain image is the calculated asymmetry between individual images (i.e. difference normalized by the sum). The sample holder contains an electromagnet that permits application of magnetic fields up to 190 Oe parallel or antiparallel to the in-plane projection of the incident x-rays for a duration of 1 second. After each field pulse, a smaller reverse field was applied to remove remanent fields in the magnetic yoke. This compensating field is at most 25% of the initial field pulse, so unwanted switching in the micromagnets does not occur. All images are captured in the remanent, zero field state.

Experimental results were compared to micromagnetic simulations performed using MuMax^3 (*15*). Unless otherwise noted, the standard inputs correspond to LSMO parameters at 100 K. These inputs include the saturation magnetization, M_S (400 kA/m), cubic magnetocrystalline anisotropy constant, K_1 (-2 kJ/m^3), and exchange stiffness, A_{ex} (3.8 pJ/m). The simulation cell volume was set to 5×5×5 nm^3 in order to

calculate the lowest energy state of a specific magnetic microstructure, in either remanence or applied fields, using the Landau-Lifshitz-Gilbert equation (*15*). Materials parameters were obtained from Lee *et al. (16)*.

Results

X-PEEM images of the bilayer sample in Figure 1 present the temperature dependence of FM/AFM spin alignment within zigzag wires with 2 μm × 0.5 μm segments oriented along the in-plane <110> directions. At all temperatures below T_C, the FM domain structure obeys shape anisotropy constraints (*i.e.* moments aligned along the segment long axis). The <110> directions also coincide with the FM easy axis in continuous LSMO films grown on (001)-oriented STO (*17*), further stabilizing the domain configuration seen in Figure 1. At elevated temperatures near and above T_C of the LSMO sublayer, the AFM domains also follow a shape-induced anisotropy, leading to parallel alignment of the FM and AFM spin axes. This observation is consistent with prior work on similarly fabricated LFO microstructures that showed shape-induced AFM domain formation resulting from structural constraints present in a patterned, epitaxial film in a surrounding non-magnetic matrix (*18*). This parallel orientation of spin axes breaks down below 200 K as the frustrated state emerges, and the LFO layer breaks down into many smaller domains approximately a few hundred nanometers in diameter aligned along [110] and [$1\bar{1}0$] directions. These respective directions correspond to the dark and light regions observed in the XMLD images of the zigzag nanowire acquired at 100 K and 200 K in Figure 1. Reducing the temperature further pushes the system fully into the spin-flop configuration, as the AFM spin axis is now always perpendicular to the FM moments and the long axis of the patterned segments. Within this experimental range, the magnetization in the LSMO layer changes considerably, from zero at 300 K to 400 kA/m at 30 K. Our results suggest that for low LSMO magnetization, the shape-induced effects dominate the AFM domain structure, while at high LSMO magnetization the exchange coupling between the FM and AFM spins prevails. These two regimes are separated by a frustrated region where a mixture of parallel and perpendicular spin alignment is found.

In order to study the magnetic switching behavior, 2 μm × 0.5 μm rectangular micromagnets were characterized from a series of X-PEEM images captured under remanent conditions between *in situ* magnetic field pulses of approximately 1 second in duration at temperatures ranging from 30 K to 200 K. The applied fields induce no observable change in XMLD images of the LFO sublayer, but 180° switching is readily seen in XMCD images of the LSMO sublayer, where the contrast switches completely from dark to light. This contrast change indicates a complete reversal of magnetization between the two stable monodomain states of the FM layer within individual micromagnets. Tallying the switching events after each field pulse allows for the construction of the magnetization switching curves shown in Figure 2(c), which are fit to a normal cumulative distribution function. No unidirectional exchange bias is observed as the switching curves are experimentally identical upon application of field pulses in the opposite direction. Coercivity of both single-layer and bilayer samples increases as the temperature decreases, but the bilayer micromagnets consistently require a greater applied field to reverse magnetization. The spread in switching fields for an individual temperature results from pattern variations and defects within the array of micromagnets. Thermally induced switching is extremely unlikely for micromagnets with these dimensions and magnetic parameters. (This phenomenon has been thoroughly addressed in the Supplementary Material from (*8*).)

Discussion

The simplest form of the Stoner-Wohlfarth model for a coupled bilayer system describes the free energy as the sum of the FM and AFM free energies in addition to the interlayer coupling term that drives the spin-flop alignment (*8*):

$$F = F_{FM} + F_{AFM} + F_{coupling}$$

The individual components are described by the following equations involving the FM layer magnetization, M_0, AFM moment, L_0, magnet volume, V, shape anisotropy fields for each layer, H_{shape}^{FM}

and H_{shape}^{AFM}, the externally applied field, H_{ext}, and the interfacial exchange coupling term, $H_{coupling}$. Angles φ_{FM}, φ_{AFM}, and θ defined in Figure 2(b) are all relative to the direction of the microstructure long axis and describe the orientation of the FM spin axis, AFM spin axis, and external field, respectively. Summations are introduced to represent the multi-domain character of the AFM layer in the frustrated alignment.

$$F_{FM} = -\frac{1}{2}M_0 V H_{shape}^{FM} cos^2\varphi_{FM} - M_0 V H_{ext}\cos(\varphi_{FM} - \theta)$$

$$F_{AFM} = \sum_i -\frac{1}{2}L_{0,i}V_i H_{shape,i}^{AFM} cos^2\varphi_{AFM,i}$$

$$F_{coupling} = \sum_i \frac{1}{2}M_{0,}V_i H_{coupling} cos^2(\varphi_{FM,i} - \varphi_{AFM,i})$$

The equilibrium orientation of the ferromagnet is the free energy minimum defined by the derivative of F with respect to φ_{FM}. This point becomes unstable as the second derivative also approaches zero under the application of an external field, leading to the magnetic reversal of the FM layer (e.g., φ_{FM} rotates from 0° to 180°). Since φ_{AFM} is constant at a specific temperature while rotating the FM moment via an applied field, the F_{AFM} term is not present in the derivatives and therefore has no influence on the equilibrium and reversal conditions. Thus, the relevant free energy landscape is determined by the characteristics of the FM layer, its response to applied fields, and the angle between the FM and the AFM spin axes used to calculate $F_{coupling}$. It can now be seen how $F_{coupling}$ modifies the energy barrier between $\varphi_{FM} = 0°$ and $\varphi_{FM} = 180°$ that must be overcome by the external field for both parallel alignment,

$$F_{coupling}^{parallel} = \frac{1}{2}M_0 V_{0°} H_{coupling} cos^2(\varphi_{FM} - 0°)$$

and spin-flop alignment.

$$F_{coupling}^{spin-flop} = \frac{1}{2}M_0 V_{90°} H_{coupling} cos^2(\varphi_{FM} - 90°)$$

Relative to the single layer LSMO, involving only F_{FM}, the parallel configuration reduces the barrier height whereas spin-flop does the opposite. In the frustrated case, where there is an equal mixture of parallel and spin-flop domains in the AFM layer, then $F_{coupling} = F_{coupling}^{parallel} + F_{coupling}^{spin-flop}$, which can be reduced to a constant and is no longer present in the derivatives that determine the equilibrium and reversal conditions.

As outlined above, aspects of Stoner-Wohlfarth theory apply to this system to guide our understanding, but rigorous, analytical calculations cannot be accurately applied. The primary complication stems from the Stoner-Wohlfarth assumption that switching occurs through coherent rotation within a fully saturated magnet. This notion is valid for structures with dimensions on the order of the material's exchange length (*19*) (approximately 6 nm for LSMO (*20*)), but the micromagnets of this study are much larger. Incoherent switching and flux-closure domains (shown in Figure 3) at the short ends of the rectangular micromagnets prevent accurate determination of H_{shape}^{FM}. It can be seen in Figure 2 that the switching field distribution width increases as temperature decreases, which is consistent with experiments on amorphous bistable magnetic microwires that are known to switch via propagation of flux-closure domain walls nucleated at wire ends pinned to atomic scale defects (*21*). MuMax[3] simulations of the LSMO micromagnets also indicate that domain wall motion plays a dominant role in their switching mode (*15*). These reversal processes dominate at the macroscopic level to determine the coercivity of these micromagnets, but aspects of Stoner-Wohlfarth theory appear to be applicable at the mesoscopic level. Namely, $F_{coupling}$ can show how structures with equivalent switching mechanisms, but different coupling interactions, should behave relative to one another. Individual FM moments are still sensitive to adjacent AFM domains during rotation and switching, even if the interplay between FM and AFM moments is not coherent throughout the micromagnet.

The data to test this hypothesis is presented in Figure 2(c), which captures the distribution of switching events as a function of applied field for the bilayer as the spin alignment transitions from parallel at 300 K towards spin-flop at 30 K alongside a similar set of curves for the FM single-layer, for reference. To more intuitively compare the switching behavior over this temperature range, Figure 4 plots the switching field defined as the value where 50% of the micromagnets have switched, as determined by the respective fit curves in Figure 2(c). At all temperatures, the bilayer requires a higher applied field to switch. Additionally, the <100> data from (*8*) has been included for a comprehensive depiction of the system.

Above 30 K, the single-layer and bilayer show the same gradual decrease in switching field with temperature, but with an offset of 10-15%. In this regime, frustrated spin alignment dominates and equivalent coercivities would be expected for the two structures. The slight offset is a result of the difference in FM thickness between the single-layer (100 u.c. LSMO) and bilayer (90 u.c. LSMO). MuMax^3 simulations show that a 90 u.c. FM micromagnet at these dimensions will switch at a field ~10% greater than the 100 u.c. layer (*15*), which suggests that the experimental switching behavior between 60 K and 200 K is consistent with a thickness-dependent effect.

The switching fields near 30 K shows a clear divergence from the trend present between 60 K and 200 K. The coercivity of the bilayer jumps to a value larger than can be accounted by the difference in LSMO layer thickness, and the X-PEEM images (*e.g.,* Figure 1) verify the spin-flop alignment emerging at 30 K that should lead to an increased coercivity. This outcome is again in agreement with the influence of the interfacial coupling component of the free energy model. Folven *et al.* found that parallel coupling in <100>-oriented micromagnets at 110 K reduced the AFM/FM bilayer switching field by 30% relative to the FM single-layer micromagnets (*8*). The spin-flop alignment that emerges at 30 K in the <110>-oriented micromagnets shown here increases the switching field by approximately 25% (after correcting for the difference in LSMO thickness).

The large difference in switching field between the <100>- and <110>-oriented micromagnets at 110 K emerges because of the remanent FM domain structure in each type of micromagnet as described by both X-PEEM data and simulated domain pattern images in Figure 3. As stated earlier, switching in this system occurs via a domain wall nucleation and propagation mechanism. Rectangular micromagnets oriented along <110> directions are likely to form vortex flux-closure domains at the ends, which greatly reduces the switching field as domain walls are already nucleated within the structure. This FM domain structure persists at 30 K in the bilayer sample despite strong spin-flop coupling to the LFO layer. Micromagnets oriented along <100> directions do not form this structure, as doing so introduces too large of a magnetocrystalline anisotropy energy cost, and domain walls must be nucleated by the applied field. It is expected that minor modifications to the pattern geometry should provide even further control over remanent magnetization states and thus coercivity.

Conclusions

In summary, we demonstrate that considerable variation in coercivity (30 to 190 Oe) takes place when the spin alignment at the FM/AFM interface in an epitaxial micromagnet is altered. Depending on the temperature and crystalline orientation of such micromagnets, parallel, frustrated, and spin-flop alignment can be stabilized. Using a combination of micromagnetic simulations and free energy modeling, the switching behavior of this complex system can be accurately characterized. While maintaining many aspects of the micromagnet constant such as crystallinity, chemistry, or fabrication conditions, our findings emphasize the sensitivity of spin alignment on material properties of the individual layers and the resulting effect on functional properties.

Acknowledgements

Funding for these experiments was obtained from the National Science Foundation (DMR 0747896 and 1411250), the Research Council of Norway (221860/F60), and the Outstanding Academic Fellows program at NTNU (E.F.). The Advanced Light Source is supported by the Director, Office of Science,

Office of Basic Energy Sciences, and the U.S. Department of Energy (DE-AC02-05CH11231). Patterning of the micromagnets was performed at the Center for Nanophase Materials Sciences, a U.S. Department of Energy Office of Science User Facility.

Declaration of interest

No authors report any competing financial interests.

***Corresponding Author**

Yayoi Takamura

Department of Materials Science and Engineering

University of California, Davis

One Shields Avenue

Davis, CA 95616

Phone: 530-754-7124

Fax: 530-752-1031

Email: ytakamura@ucdavis.edu

Figures

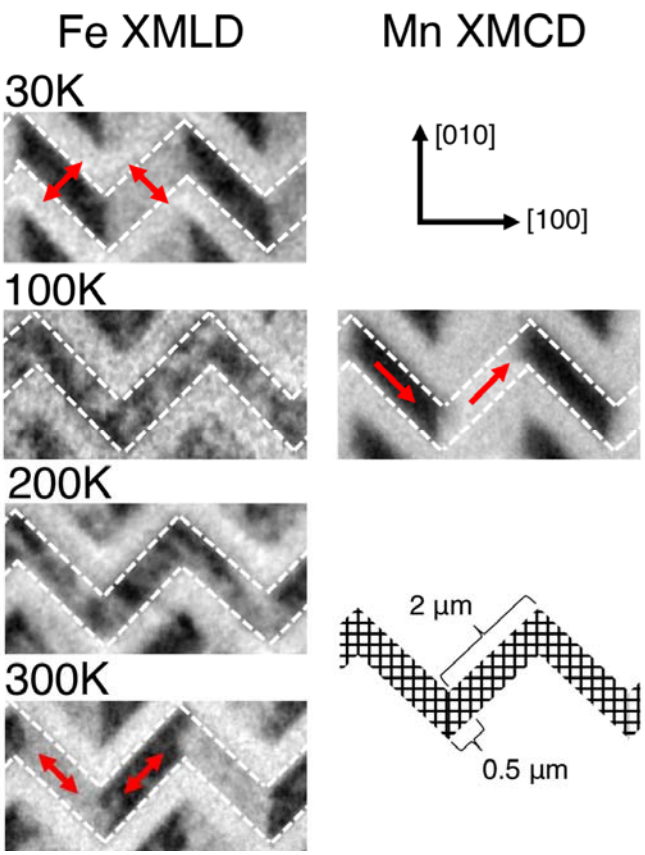

Figure 1: (Left column) XMLD images of the LFO layer in the zigzag wires at temperatures between 30 K, where the AFM spin axis is perpendicular to the wire edge (spin-flop), through frustrated alignments at 100 K and 200 K, to 300 K, where the AFM spin axis becomes parallel to the wire edge. (Right column) Crystallographic legend, XMCD image of the LSMO zigzag wire at 100 K with FM domains oriented parallel to edges of the wire, and a schematic of nanowire dimensions. The incident x-rays are along the $[1\bar{1}0]$ direction for all X-PEEM images.

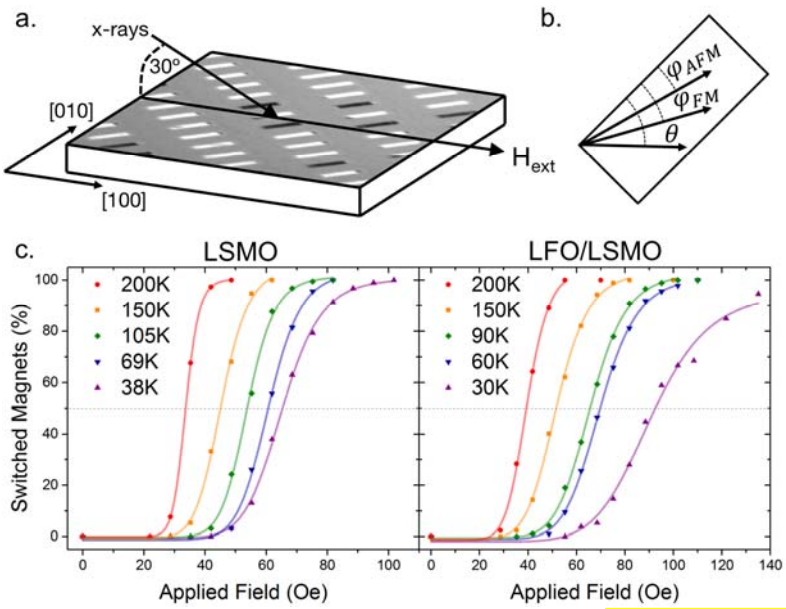

Figure 2: (a) XMCD image of a partially switched (<110>-oriented, LSMO single layer at 105 K after applied field of 49 Oe) micromagnet array combined with schematic of the X-PEEM experimental setup depicting the incident x-ray angle, micromagnet orientation, and applied field direction. (b) Angles for applied field H_{ext}, FM spin axis φ_{FM}, and AFM spin axis φ_{AFM} defined relative to the long axis of the individual micromagnets. (c) Percentage of micromagnet array switched *vs.* applied field for the LSMO single-layer (left) and LFO/LSMO bilayer (right) samples at temperatures between 30 K and 200 K. Solid lines are normal cumulative distribution function fits, and the intersection with the horizontal dashed line corresponds to the field where 50% of micromagnets have switched.

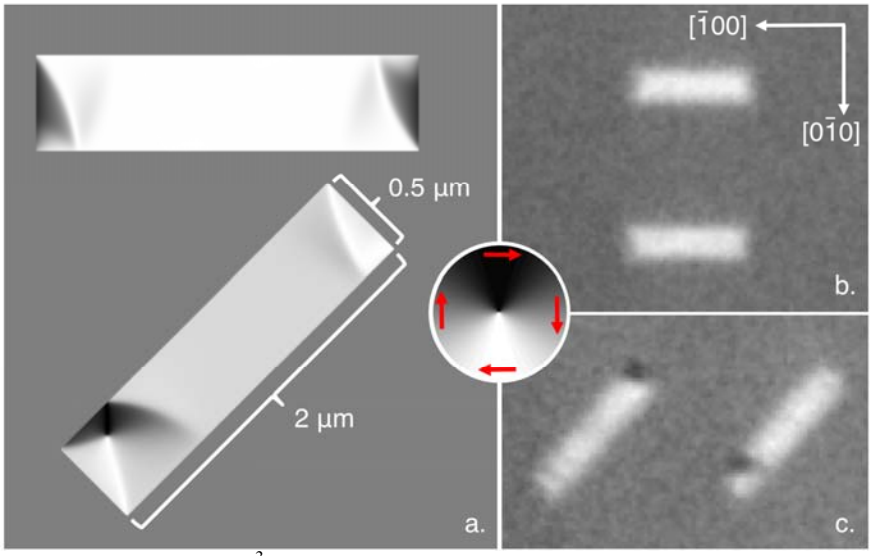

Figure 3: (a) MuMax[3] simulations of saturated, remanent state for both <100> (top) and <110> (bottom) oriented micromagnets showing the presence and absence of a vortex flux-closure domain in the <100> and <110> structures, respectively. (b) XMCD image of <100> oriented micromagnets. (c) XMCD image of <110>-oriented micromagnets at 100 K. Both (b) and (c) show only two 2 µm × 0.5 µm rectangular structures from an array of ~100.

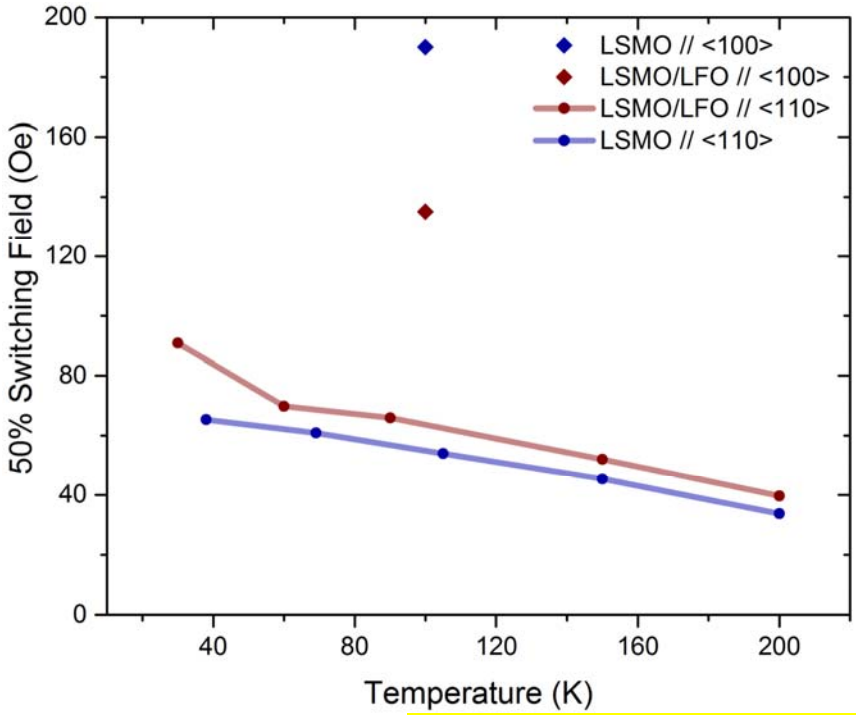

Figure 4: 50% switching field for 2 μm × 0.5 μm rectangular micromagnet arrays plotted as a function of temperature. Blue corresponds to single-layer LSMO and red to LFO/LSMO bilayer samples. Data collected in this study on micromagnets with long edges parallel to <110> are represented by circles. The <100> data included from (*8*) are denoted by diamond symbols.

References

1. J. Nogues, I. K. Schuller, Exchange bias. *J. Mag. Mag. Mater.* **192**, 203-232 (1999).
2. F. E. Luborsky, Development of Elongated Particles. *Journal of Applied Physics* **32**, S17 (1961).
3. Y. T. Shen, Y. H. Wu, H. Xie, K. B. Li, J. J. Qiu, Z. B. Guo, Exchange bias of patterned NiFe/IrMn film. *Journal of Applied Physics* **91**, 8001-8003 (2002).
4. R. L. White, Review of Recent Work on the Magnetic and Spectroscopic Properties of the Rare-Earth Orthoferrites. *J. Appl. Phys.* **40**, 1061-1069 (1969).
5. N. C. Koon, Calculations of Exchange Bias in Thin Films with Ferromagnetic/Antiferromagnetic Interfaces. *Phys. Rev. Lett.* **78**, 4865-4868 (1997).
6. L. L. Hinchey, D. L. Mills, Magnetic properties of ferromagnetic-antiferromagnetic superlattice structures with mixed-spin antiferromagnetic sheets. *Phys. Rev. B* **34**, 1689-1699 (1986).
7. E. Folven, A. Scholl, A. Young, S. T. Retterer, J. E. Boschker, T. Tybell, Y. Takamura, J. K. Grepstad, Crossover from Spin-Flop Coupling to Collinear Spin Alignment in Antiferromagnetic/Ferromagnetic Nanostructures. *Nano Letters* **12**, 2386-2390 (2012).
8. E. Folven, J. Linder, O. V. Gomonay, A. Scholl, A. Doran, A. T. Young, S. T. Retterer, V. K. Malik, T. Tybell, Y. Takamura, J. K. Grepstad, Controlling the switching field in nanomagnets by means of domain-engineered antiferromagnets. *Physical Review B* **92**, 094421 (2015).
9. A. Scholl, J. Stohr, J. Luning, J. W. Seo, J. Fompeyrine, H. Siegwart, J.-P. Locquet, F. Nolting, S. Anders, E. E. Fullerton, M. R. Scheinfein, H. A. Padmore, Observation of antiferromagnetic domains in epitaxial thin films. *Science* **287**, 1014-1016 (2000).
10. J. F. Ziegler, M. D. Ziegler, J. P. Biersack, SRIM – The stopping and range of ions in matter (2010). *Nuclear Instruments and Methods in Physics Research B* **268**, 1818-1823 (2010).
11. Y. Takamura, R. V. Chopdekar, A. Scholl, A. Doran, J. A. Liddle, B. Harteneck, Y. Suzuki, Tuning magnetic domain structure in nanoscale $La_{0.7}Sr_{0.3}MnO_3$ islands. *Nano Letters* **6**, 1287-1291 (2006).
12. E. Folven, Y. Takamura, J. K. Grepstad, X-PEEM study of antiferromagnetic domain patterns in $LaFeO_3$ thin films and embedded nanostructures. *J. Electron Spectrosc. Relat. Phenom.* **185**, 381-388 (2012).
13. S. Anders, H. A. Padmore, R. M. Duarte, T. Renner, T. Stammler, A. Scholl, M. R. Scheinfein, J. Stohr, L. Seve, B. Sinkovic, Photoemission electron microscope for the study of magnetic materials. *Rev. Sci. Instrum.* **70**, 3973-3981 (1999).
14. J. Stohr, S. Anders, X-ray spectro-microscopy of complex materials and surfaces. *IBM Journal of Research and Development* **44**, 535-551 (2000).
15. A. Vansteenkiste, J. Leliaert, M. Dvornik, M. Helsen, F. Garcia-Sanchez, B. Van Waeyenberge, The design and verification of MuMax3. *AIP Advances* **4**, 107133 (2014).
16. M. S. Lee, T. A. Wynn, E. Folven, R. V. Chopdekar, A. Scholl, A. T. Young, S. T. Retterer, J. K. Grepstad, Y. Takamura, Tailoring Spin Textures in Complex Oxide Micromagnets. *ACS Nano* **10**, 8545-8551 (2016).
17. L. M. Berndt, V. Balbarin, Y. Suzuki, Magnetic anisotropy and strain states of (001) and (110) colossal magnetoresistance thin films. *Appl. Phys. Lett.* **77**, 2903-2905 (2000).
18. E. Folven, T. Tybell, A. Scholl, A. Young, S. T. Retterer, Y. Takamura, J. K. Grepstad, Antiferromagnetic Domain Reconfiguration in Embedded $LaFeO_3$ Thin Film Nanostructures. *Nano Letters* **10**, 4578-4583 (2010).
19. A. Hubert, R. Schafer, *Magnetic Domains—The Analysis of Magnetic Microstructures*. (Springer, Berlin, New York, Heidelberg, 1998).
20. G. S. Abo, Y. K. Hong, J. Park, J. Lee, W. Lee, B. C. Choi, Definition of Magnetic Exchange Length. *IEEE Transactions on Magnetics* **49**, 4937-4939 (2013).
21. R. Varga, K. L. García, M. Vázquez, A. Zhukov, P. Vojtanik, Switching-field distribution in amorphous magnetic bistable microwires. *Physical Review B* **70**, 024402 (2004).